The urban wind island from a three-dimensional perspective

Droste, A. M.; Holtslag, A. A.M.; Steeneveld, G. J.

DOI
10.1016/j.uclim.2024.102164

Publication date
2024

Document Version
Final published version

Published in
Urban Climate

Citation (APA)
Droste, A. M., Holtslag, A. A. M., & Steeneveld, G. J. (2024). The urban wind island from a three-dimensional perspective. *Urban Climate*, *58*, Article 102164. https://doi.org/10.1016/j.uclim.2024.102164

Urban Climate 58 (2024) 102164

Contents lists available at ScienceDirect

Urban Climate

journal homepage: www.elsevier.com/locate/uclim

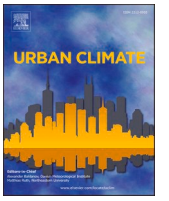

The urban wind island from a three-dimensional perspective

A.M. Droste [a,b], A.A.M. Holtslag [b], G.J. Steeneveld [b,*]

[a] Department of Water Management, Faculty of Civil Engineering, Delft University of Technology, Delft, P.O. Box 5048, 2600 GA Delft, the Netherlands

[b] Meteorology and Air Quality Section, Wageningen University and Research, Wageningen, PO Box 47, 6700 AA, the Netherlands

ARTICLE INFO

Keywords:
Urban boundary layer
Wind speed
WRF model
Urban wind island

ABSTRACT

The Urban Wind Island (UWI), a small but persistent positive mean boundary-layer wind anomaly over the city as a whole, has previously been revealed using a simplified conceptual model of the convective atmospheric boundary layer. This study extends the UWI research into less idealised cases by using the three-dimensional WRF mesoscale model for Amsterdam (The Netherlands) and its surroundings, at 500 m grid spacing. Two summers of forecast results for in total 173 days are used to identify whether the UWI persists in a three-dimensional modelling environment, and which conditions are optimal for its formation and persistence. In order to focus only on wind modified by surface processes, large-scale influences which modify wind speed, such as frontal passages, are identified and eliminated from the dataset. We then find that a positive UWI is present roughly half the time, with an order of magnitude that is similar to the previous work ($\sim$ 0.2–0.5 ms^{-1}). In addition we find an evening UWI that is caused by the delayed onset of the transition from an unstable to a stable or a neutral boundary layer in the urban area, while the rural area is already stable and calm.

1. Introduction

Currently, more than half of the world population lives in cities and this amount is expected to keep rising (U. N. D. of Economic, S. Affairs, Urban and Rural Population Growth and World Urbanization Prospects. World Urbanization Prospects: The, 2018). It is therefore important to investigate how a livable environment for this urban population can be created and maintained. Cities have their distinct environmental challenges, such as excess heat (e.g. Nazarian et al., 2022), relatively poor air quality (e.g. Zhang et al., 2022), and wind nuisance (Oke et al., 2017). At present, several challenges appear in understanding the physics and dynamics of the complex urban microclimate. Within a neighbourhood or even a single street canyon, strong contrasts in air and surface temperatures, wind speed and radiation are the norm, rather than the exception. Due to this strong heterogeneity, taking representative urban meteorological measurements is extremely challenging and a costly affair. Though human activity concentrates in cities, routine meteorological measurement sites are exclusively situated in rural areas, that are preferably flat and homogeneous to capture the undisturbed larger-scale meteorological background required for accurate large-scale weather forecasting. Some weather stations have even been moved further away from encroaching urban sprawl (Yang et al., 2013; Bassett et al., 2019), lest it "contaminates" the rural background with the enhanced heat or roughness so typical of the urban environment.

The understanding of wind in urban areas is of particular interest for the understanding and prediction of air pollution transport

* Corresponding author.
E-mail address: Gert-Jan.Steeneveld@wur.nl (G.J. Steeneveld).

https://doi.org/10.1016/j.uclim.2024.102164
Received 22 September 2023; Received in revised form 7 August 2024; Accepted 7 October 2024
Available online 17 October 2024

(Fallmann et al., 2016; Azargoshasbi et al., 2023), ventilation of urban heat (Jing et al., 2021; Biehl et al., 2021; Karlický et al., 2018) and for urban wind energy production (Micallef and Bussel, 2018). At the street scale, the wind speed and direction and the turbulence at street level is strongly governed by the street profile properties (e.g. aspect ratio) and orientation. Classically we distinguish between skimming flow for high aspect ratios and wake interference flow for relatively low aspect ratios. In skimming flow the wind above the canyon is more or less decoupled from the wind in the canyon, while in the latter the wind can enter the street canyon to a certain degree.

However, this study focuses on the mean planetary boundary layer (PBL) wind which depends on the geostrophic wind speed driven by the large-scale synoptic conditions and by the drag provided by the roughness of the city (Lee, 1967; Bornstein and Johnson, 1967). Considering its diurnal cycle, in the early morning the rural wind speed is slightly higher than the urban wind speed. Then during daytime the PBL grows over both the rural and urban surfaces under the influence of increasing surface sensible heat flux, and entrainment of warm and high-momentum air from the free atmosphere. The relatively rough urban surface creates drag and takes out momentum, and slows down the flow, which creates an ageostrophic wind speed. For relatively long days this ageostrophic wind speed might interact with the Earth's rotation (Coriolis parameter). However, the precise interaction between the surface drag (through turbulence), the entrainment and lateral advection of momentum, and the geostrophic wind speed over cities is still not understood (Barlow, 2014; Tsiringakis et al., 2022).

In an earlier study Droste et al., 2018 (henceforth *D18*) compared the daytime boundary-layer wind evolution in urban and rural boundary layers (Fig. 1) as modelled with a bulk model for the convective boundary layer. They found that the contrasting PBL dynamics between city and countryside can surprisingly induce an urban wind island (UWI): i.e. a positive difference in PBL-averaged wind speed between urban and rural areas. The main mechanism behind the UWI is an oscillation of the mean PBL ageostrophic wind speed around the geostrophic wind speed. The ageostrophic wind at the start of the day causes a larger amplitude of the oscillation in the city than in the countryside (overshoot). The larger amplitude of the urban oscillation causes the urban wind to accelerate for a longer period of time, thereby forming the UWI. D18 found that the UWI disappears for non-rotating flows, and that the UWI remains visible for equal roughness lengths over city and countryside, and that the UWI magnitude strongly increases when entrainment is absent.

The D18 study found the UWI for ideal urban and rural atmospheric columns that did not communicate with each other. Therefore this study aims to identify whether the UWI phenomenon manifests itself in a three-dimensional context as well, and as such might be present in the real world too. Since urban wind observations are challenging, especially of a PBL averaged phenomenon such as the UWI, we use a hectometric mesoscale modelling approach (Barlow et al., 2017; Ronda et al., 2017). Such an approach allows for representing cities with a relatively large amount of grid cells and thus for representing spatial contrasts in land use and urban morphology, and for approximately realistic city borders. This approach is preferred over using relatively coarse regional climate model results that lack spatial detail in the city representation. Currently utilized model results are based on the WRF model (Weather Research & Forecasting, (Skamarock et al., 2008; Powers et al., 2017)) at very fine grid spacing (100 m at the inner domain) with improved urban physical schemes and land-use properties for Amsterdam, The Netherlands. Using the model results for two summers, 2017 and 2018, we study whether the UWI occurs in these model results, which conditions are optimal to its formation, and what similarities or differences these have with respect to the theory of *D18*.

This paper is organised as follows: Section 2 provides background information about the wind dynamics and the UWI, Section 3 introduces the model setup, study area and research strategy; Section 4 provides the results, looking at UWI statistics under various conditions, its time of formation, and role of initial conditions; Section 5 discusses the implications of the results and Section 6 answers the research questions.

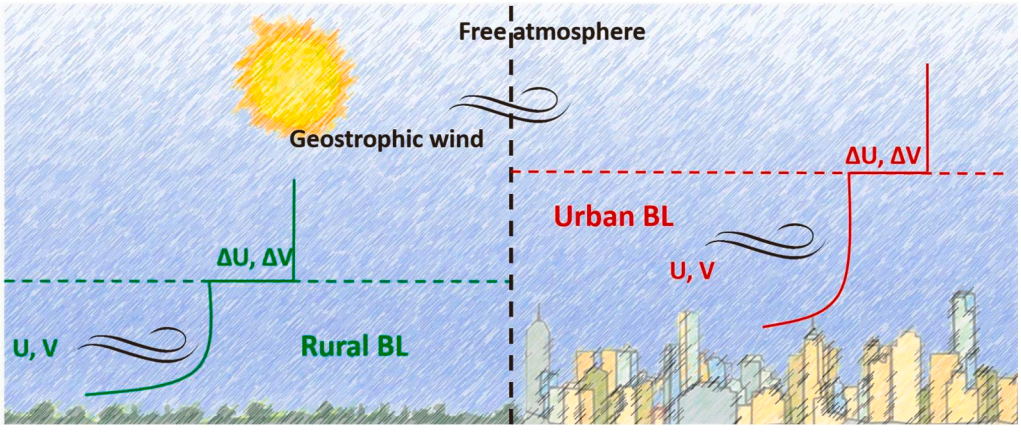

Fig. 1. Schematic overview of the conceptual model used in (Droste et al., 2018). The urban and rural part of the model do not communicate, but are influenced by the same geostrophic wind speed.

2. Background

The wind dynamics in the PBL follows the budget equations for momentum, here illustrated for a bulk model (excluding subsidence):

$$dU/dt = f(V - V_G) + \left(< uw >_0 - < uw >_{top} \right)/h \quad (1)$$

$$dV/dt = -f(U - U_G) + \left(< vw >_0 - < vw >_{top} \right)/h \quad (2)$$

$$d\Delta U/dt = w_e \gamma_U - dU/dt \quad (3)$$

$$d\Delta V/dt = w_e \gamma_V - dV/dt \quad (4)$$

$$< uw_{top} > = -w_e \Delta U \quad (5)$$

$$< vw_{top} > = -w_e \Delta V \quad (6)$$

Herein U and V are the longitudinal and meridional PBL mean wind speed components (ms^{-1}), U_G and V_G the components of the geostrophic wind speed (ms^{-1}), h the time dependent PBL depth (m), w_e the entrainment velocity (ms^{-1}), ΔU and ΔV the wind speed jumps at level h (ms^{-1}), $< uw_0 >$ and $< uw_{top} >$ (in $m^2 s^{-2}$) the momentum fluxes at the surface and PBL top respectively, and f the Coriolis parameter s^{-1}.

This mixed-layer model is a bulk-representation of the PBL, with influences from the underlying surface and the free troposphere above. In *D18*, two separate columns have been modelled, with the same free atmosphere, but with distinct homogeneous surface properties for each column, either urban or rural. With this set-up a positive wind difference between the urban and rural column can be found under certain circumstances (clear-sky days with moderate wind speeds): the UWI.

In the analysis of the D18 model results, the two driving factors of the UWI appeared to be the ageostrophic wind speed magnitude (the difference between the geostrophic wind speed, and the mean PBL wind speed), and the difference in the PBL depth between urban and rural areas at the start of the day. The UWI is a relatively small effect, with magnitudes up to 0.5 ms^{-1} found in *D18*. Hence, it stands to reason that under the idealised circumstances of the conceptual model used, the UWI might not persist if other local processes are dominant. On the other hand, also observational evidence of the UWI has been provided (Fortuniak et al., 2006), which suggests that the UWI is a real phenomenon, distinct from the sharp microscale differences in wind speeds often observed near buildings (canyon tunnelling or wind lulls at the leeward side of obstacles).

D18 found the most favourable conditions for UWI formation to be a moderate geostrophic wind speed ($\sim$ 5 ms^{-1}), a positive difference in PBL depth between urban and rural at sunrise, and cloudless conditions which encourage strong PBL development dominated by local effects. Note that outside of the idealised conditions for which the boundary conditions can be controlled, frontal effects and other mesoscale phenomena may also influence the wind fields in both urban and rural areas, which can cause wind differences between the two that should not be considered an UWI. Thus, we narrow our definition of an UWI to be *"a positive wind difference between an urban and nearby rural area, caused by differences in local dynamics"*, and therefore need to remove large-scale effects that could suggest an UWI where there is none.

3. Methodology and data

First, section 3.1 introduces the utilized WRF model setup for the study area of Amsterdam and its surroundings. Additionally, a single day is selected to illustrate the UWI formation (section 4.2), based on the favourable conditions for the UWI as found by *D18*. The data analysis strategy to outline potential causes of the UWI is presented in section 3.2.

3.1. WRF model setup and study area

Our area of interest is the city of Amsterdam, with its center point at 52.373° N, 4.892° E, in the north-west of The Netherlands, and its rural surroundings. The region is characterised by a temperate maritime climate (Köppen Cfb climate) with the IJssel Lake in the vicinity ($\sim$ 8 km) to the east and the North Sea ($\sim$ 30 km) to the west.

The WRF model (version 3.7.1) has been run for the study area with a customised land-surface and urban physics scheme as in

Table 1
Overview of WRF model domain and grid setup.

Domain	Domain size (m)	Domain size (m)	Grid (m)	Central	Central	Time step (s)
	North-South	East-West	size	latitude	longitude	
d01	1487.5	1487.5	12,500	51.964	5.663	60
d02	300	300	2500	52.374	4.820	12
d03	60	60	500	52.351	4.896	2.4
d04	17.5	13.5	100	52.352	4.907	0.48

Ronda et al. (2017), which forms the core dataset of this work. The model setup contains 4 one-way nested domains (Table 1), each increasing with a factor 5 in grid spacing, from 100 m of the inner (4^{th}) domain up to 12.5 km for the outer domain, roughly comprising north-western Europe. The WRF forecasts have been driven by GFS operational global forecasts initialised at 00:00 UTC, and have a lead time of 48 h, of which the first 24 h are considered as spin-up. The selected physical parameterizations used are summarized in Table 2, and this configuration is justified by model validation results reported in (Ronda et al., 2017). Soil- and urban fabric temperatures are initialised from the previous forecasts, and water temperatures for the two inner domains are taken from observations by Rijkswaterstaat (Directorate-General for Public Works and Water Management): the governmental water body and infrastructure managing agency. Ronda et al. (2017) focus their analysis on the inner, 100 m grid spacing domain which is mainly the inner city of Amsterdam. Since this domain does not comprise of a rural area to serve as reference, we uniquely analyse the model results of the 500 m grid spacing *3rd* domain, centred on Amsterdam, which encompasses a large amount of the western Netherlands, including a swath of rural land to the south and north of Amsterdam (Fig. 2).

To identify a robust urban wind signal, we analyse model results in as a grid-average of a 5 × 5 grid-cells area (2.5 km × 2.5 km) in the city centre, which is distant from the city borders and large water bodies. Selecting the rural reference location is challenging, since undisturbed rural areas are virtually absent to the east and west of Amsterdam, with various cities to the west and the IJssel-lake to the east. Ideally, the rural reference wind speed would be upwind of the city, so no plume effects or momentum changes are advected from the relatively rough urban area to the rural reference, essentially "polluting" the rural signal which needs to be clear of urban influence.

The area north of Amsterdam contains some urban structures, and the south is bordering a large nature reserve with well-watered meadows. Since the southern reference is quite far (25 km) from the city center, it is likely that any urban influence will already be dispersed by the time air parcels reach the location in case of northerly winds. Hence, the UWI could be independent of wind direction, using a fixed reference location instead, since the only other option would be the northern area, and northerly winds occur infrequently in the Dutch climate (Sluiter, 2011). In section 4.1 we first show that indeed we can use this fixed reference even during northerly winds. A grid-average of 5 × 5 cells is also used for the rural wind values. Since we use a grid-average instead of a single grid point, the exact location of the 5 × 5 grid is not crucial. Sensitivity tests have shown that moving the 5 × 5 grid 1 or 2 model grid cells along the north-south or east-west direction results in averaged wind speed that are consistent, which indicates the robustness of the findings.

3.2. Data analysis strategy

In the introduction, we distinguished between locally created wind differences (the UWI) and larger-scale influences which could cause a spurious UWI. Frontal effects, rain causing local downbursts, or storms can all modify the wind at either the urban or rural area (or both), without the surface playing any role. To study the pure UWI, these circumstances need to be identified and removed, by utilising some of the parameters present in the WRF model results. Hence, the presence of clouds and their impact on surface radiation, the PBL depth, boundary-layer stability, and the geostrophic wind speed are all expected to contribute to UWI formation, and are extracted or calculated from the WRF output variables for selection purposes:

1. Rain is accounted for by the modelled accumulated grid precipitation, which tracks how much precipitation reaches the ground for a given grid cell over the course of that model run. If this is non-zero for the analysed day (the second day in the 48 h forecasts), it has rained, and the entire day is flagged as such. We subdivide the rain flag into 3 classes: a 0 for no or very little rain (<= 0.1 mm), a 1 for rain between 0.1 and 1.0 mm, and 2 for anything above 1 mm rain. WRF typically struggles with the timing and spatial distribution of rain, and this model setup was not validated for precipitation. However, we are not concerned with the accuracy of the modelled rain, rather how it impedes the modelled wind speed. Therefore, whether the modelled rain values are correct is not is not very important: rather that we can filter out days with (heavy) rain.
2. The geostrophic wind speed is not a direct output variable in WRF. Therefore, we estimate it from the geopotential field following (Wallace and Hobbs, 2006), at various levels. Since the model grid spacing is relatively small, our estimation is liable to induce numerical noise if we do not average over a relatively large field. Hence, we use the geopotential gradient over 25 grid cells to estimate the geostrophic wind positioned over the city centre. The geostrophic wind is here calculated from the geopotential gradient at approximately 900 hPa.
3. Thermodynamic stability of the surface layer is approximated using the bulk Richardson number ($Ri_{b,sl}$) between the surface and the first model level (approx. 30 m), which can be estimated from WRF model results in a straightforward manner ($Ri_b = g(\Delta\Theta/\Theta)\Delta z/\left(\Delta U^2 + \Delta V^2\right)$ (Eq. 5.6.3 in (Stull, 1988))). We approximate static stability by the sign of the $Ri_{b,sl}$: determining the layer as stable when $Ri_{b,sl}$ is positive, and unstable when it is negative. We also use this Ri_b to determine the PBL depth, using the parcel

Table 2
Overview of used WRF physical parameterization schemes.

Scheme	Reference
Boundary-Layer scheme (d1 and d2 only)	YSU (Hong et al., 2006)
Convection Scheme (d1 only)	Kain Fritsch (Kain, 2004)
Shortwave Radiation scheme	RRTMG (Iacono et al., 2008)
Longwave Radiation Scheme	RRTMG (Iacono et al., 2008)
Microphysics scheme	WSM3 (Hong and Lim, 2012)
Land surface scheme	NOAH (Ek et al., 2003)
Surface-layer scheme	MM5 (Jiménez et al., 2012)
Urban canopy scheme	Single-Layer Urban Canopy scheme (Chen et al., 2011)

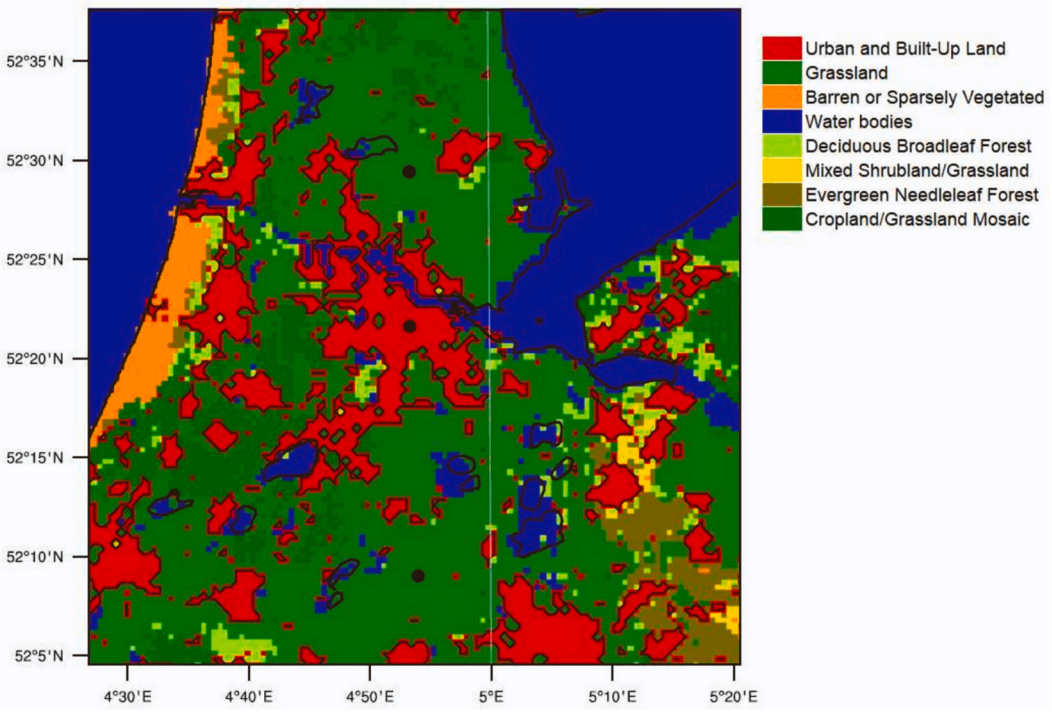

Fig. 2. Utilized land use map in the WRF model (domain 3), centred on Amsterdam. The black dot 13 km north of the city centre (52.49 N, 4.89E) and 25 km south of the city centre (52.15 N, 4.90E) mark areas designated as potential rural reference points, while the dot in the urban centre denotes the urban grid used.

method (Vogelezang and Holtslag, 1996), with the critical value of Ri_b set at 0.25. At night, we approximate the PBL depth by $h = 700u_*$ (u_* being the modelled surface friction velocity in ms^{-1}) as was proposed by (Vogelezang and Holtslag, 1996; Koracin and Berkowicz, 1988; Steeneveld et al., 2007), while during the day the maximum of the two methods is selected as the returned PBL depth. WRF does provide a PBL estimation itself but especially at night this leads to unrealistically low PBL depths, and therefore we apply an alternative method.

4. The wind speed magnitude is the vector sum of the WRF outputted u and v components of the wind speed at all model levels inside the PBL. The UWI is then the difference between the PBL-averaged wind speeds of the urban and the rural model locations. Hitherto the wind speed magnitude was averaged vertically (accounting for the mass and difference thickness of grid cells in the column) between the surface and the PBL height, and subsequently averaged over all 25 grid cells in the study areas.

Aided by these identifiers, we construct histograms of the modelled UWI for various conditions, to identify under which circumstances the UWI is highest, how long it persists (in terms of a continuous positive UWI episode) and during what time of the day the UWI occurs. We also examine whether the influence of the (initial) PBL depth is similar as in *D18*. Additionally, we explore the relation with the geostrophic wind (components) to the value of the maximum daily UWI values.

4. Results

First, we present the data analysis results, starting with a justification for the selected rural reference location in the model. Subsequently, the mean UWI is analysed with special attention to the effects of rain and stability forming the nocturnal UWI. Finally, the effect of the initial boundary-layer conditions on the UWI (PBL depth, UHI and geostrophic wind speed) are investigated.

4.1. Rural reference location

We first evaluate whether a fixed (wind direction independent) rural reference area can be used, even for situations where the receptor point is downwind from the city, and therefore potentially contaminated by the urban plume. The period between 20 and 28 July 2018, had predominantly northerly winds, varying between north-west and north-east. For that episode, 185 h of model results are available for analysis, after removing some hours where a sea-breeze front was present. The modelled UWI is calculated for both the northern (upwind) and southern (downwind) rural reference area (Fig. 2). If the difference in UWI between north and south sites is not statistically significant (using a 2-sided Student *t*-test of the difference), both sites are equally usable under these conditions, even when a site is downwind from the city. An insignificant result would suggest that this urban influence is minimal at this distance (about 20 km) and can therefore be ignored, and the southern site used as reference regardless of wind direction.

It appears the results of the statistical test are strongly insignificant: with $p = 0.769$ ($t = -0.294$; df = 338.18) we cannot reject the null hypothesis at $\alpha = 0.05$. Ergo, the mean difference between the results for the two sites is likely zero, and there is no distinguishable urban plume effect on the downwind wind speed at the southern site. Based on this result we will use the southern site as rural reference for any results from here onwards.

4.2. Convective case example

D18 showed that the UWI is most prominent on clear-sky, convective summer days with moderate large-scale wind speed, i.e. days that also tend to have relatively high UHI values. For example, August 18, 2018, was a hot day that met these criteria. WRF model results for the UWI show a similar typical evolution of the UWI as by the conceptual model of *D18* (Fig. 3). The UWI first emerges during the morning and peaks during the afternoon (with a magnitude of $\sim$0.6 ms^{-1}, consistent with earlier model results in *D18*), after which it decreases as it becomes night-time.

In addition, the UWI peaks again during the evening (20:00 UTC, or 22:00 LT) around sunset. This hints at a separate physical mechanism for the UWI, related to onset of the stable boundary layer. Rather, we hypothesise it is the delayed transition towards the urban stable boundary layer: due to the high heat storage of the urban fabric, more energy is available to drive turbulence, even when insolation is low or absent. This energy reserve is the main driver of the UHI, and also causes a delayed transition towards a more stable (neutral) boundary layer. Thus, a timeframe exists where the rural boundary layer is already stable while the urban boundary layer is not yet, which could generate a UWI until the urban boundary layer becomes stably stratified as well. Section 4.4 will explore the influence of atmospheric stability on the formation of a UWI during the evening and early night.

4.3. Mean UWI under various conditions

A histogram of the hourly UWI values over both summers (no filters) shows that the UWI values are roughly normally distributed, centred around zero, with both positive and negative outliers, favouring generally small positive UHI values (Fig. 4). Some extreme values lie beyond the plotted range: these consist of only 17 h out of a total 4152, and coincide with frontal passages. The positive UWI as modelled by WRF is generally within the range found in *D18*, about 0.5–1 ms^{-1}, with some distinct outliers going up to 2 ms^{-1}. Negative UWI seems to occur mostly at night-time (also indicated in Fig. 3), where the rural area might experience a low-level jet, or the high roughness of the urban area has a strong effect on the PBL wind speed, since the PBL depth is much lower than during the day.

When subdividing the dataset into the 3 rain categories as described in section 3.2, it initially seems that daily maximum UWI increases with the accumulated precipitation for that day. Convective precipitation events can include downbursts, i.e. modifications of the wind field due to non-local phenomena. These events are therefore better disregarded, as they do not represent the surface-induced UWI. Rain flag category 1 however, contains little precipitation (0.1 up to 1 mm day^{-1}) which is typically not associated with heavy wind activity. Possibly warm fronts, accompanied by drizzle, affect the wind field by altering the wind direction. For the rest of this study, days with >1 mm accumulated precipitation are disregarded, leaving a total of 106 days up for analysis (61% of the original dataset).

Fig. 5a shows the averaged diurnal UWI time series for those days without rain (69 days in total, 40% of the original dataset; 1656 h). The red line in Fig. 5a is the conceptual model of *D18*, run for the average forcings of the 2 years of WRF outcomes, resulting in a very similar course of UWI between the bulk model and the three-dimensional WRF model. The modelled daytime UWI values by WRF (blue line) show a strong similarity to the course of the UWI in *D18*, which also reaches its maximum at the end of the afternoon. A difference is that the UWI in this data already starts positive a little after sunrise (which is around 4:00 UTC, 6:00 LT), whereas the UWI in *D18* did not become positive before 10:00 LT (8:00 UTC). The value of this mean UWI is rather low (0.2 ms^{-1}), but realize this contains all days with the right rain flag, rather than an idealised case. The control case of *D18* also showed UWI values around 0.3 ms^{-1}, and only under more optimized circumstances did that value increase. The similarity between the three-dimensional WRF results and the mixed-layer model of *D18* suggests that on average, the UWI is formed by the core processes described in *D18*, but individual

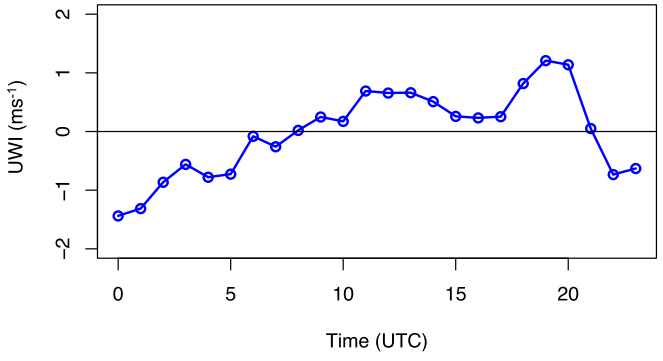

Fig. 3. Time series of modelled hourly PBL-averaged UWI over Amsterdam (The Netherlands) on August 18th, 2018. Time is in UTC (LT = UTC + 2). The southern point (Fig. 2) is used as rural reference to calculate the UWI.

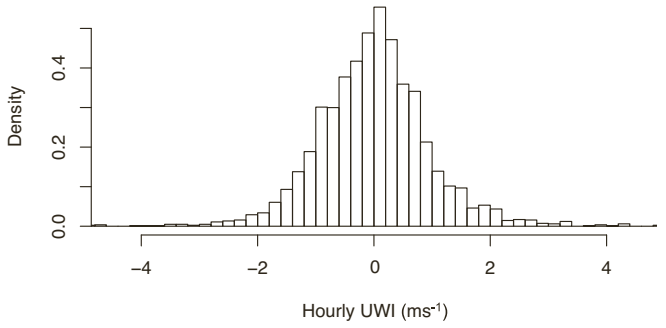

Fig. 4. Histogram of the modelled hourly UWI over Amsterdam for the selected hours in summers 2017 and 2018. Each bin is 0.2 ms^{-1} wide, totalling 4135 h.

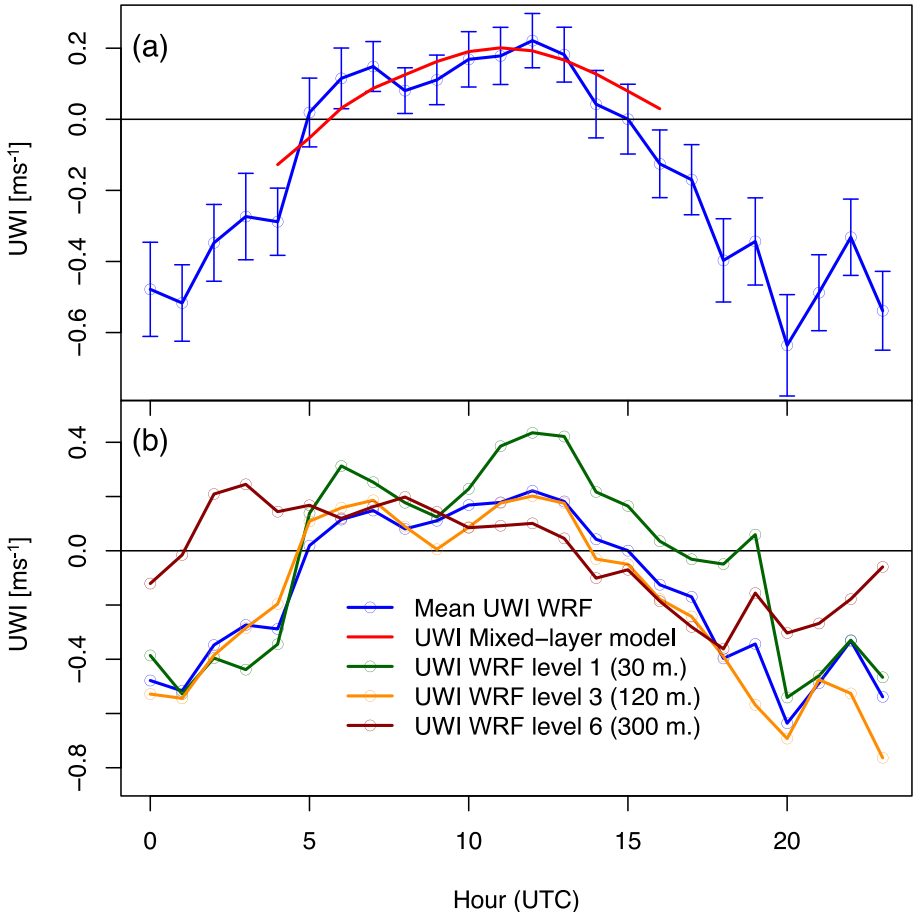

Fig. 5. a) Modelled (WRF) mean hourly UWI for Amsterdam calculated over selected days without rain (blue line) and mixed-layer model results with averaged forcings over those days (red line). Vertical error bars in a) indicate the standard error. Panel b) shows the modelled mean hourly UWI at various model levels, and the PBL-averaged UWI, which equals to that in panel a). (For interpretation of the references to colour in this figure legend, the reader is referred to the web version of this article.)

days see a strong spread in UWI formation and values.

The UWI is a PBL-averaged phenomenon, and though wind is generally a well-mixed quantity in the convective boundary layer, in practice there will be differences with height, e.g. related to wind shear. Fig. 5b also includes the UWI calculated from 3 different model levels, aside from the boundary-layer averaged UWI also shown in Fig. 5a. The first model level is at 32 m above the surface; model level 3 is at 120 m; and model level 6 at 300 m, meaning it will occasionally be above the PBL depth during early morning or late at night. Especially the surface-level UWI is more variable during the day, likely due to turbulence in the urban area generating higher

wind speeds. At night, the UWI at 300 m is positive which could be caused by low-level jets. The medium level UWI shows very similar behaviour to the PBL-weighted UWI, which is less directly reliant on the surface processes but still within the nocturnal boundary layer.

The hodograph of the average wind time series data (Fig. 6) separates the PBL-averaged wind speed into its u and v components for the urban and rural location. We indeed find a typical inertial oscillation of the wind speed over the day, turning clockwise. This is precisely the behaviour found in *D18* and also in other studies of the inertial oscillation (Blackadar, 1957; Byun and Arya, 1967; van de Wiel et al., 2010), now also extending towards night-time rather than only the convective boundary layer. Note that this is the average wind over two summers of data: individual days have quite some variability between them and may not portray an oscillation at all or only for a certain portion of the day. Similarly, the diurnal UWI evolution also shows a lot of spread over the 2 years (see the histogram in Fig. 4).

4.4. Stability and night-time UWI

As seen in the case of Fig. 3 and various other days, the UWI can be positive shortly after sunset, which the conceptual study in *D18* does not cover. During this time of the day, the PBL transitions from unstable to stable stratification, which suppresses buoyancy-driven turbulence and generally lowers the wind speed. However, the majority of positive UWI values does not occur during this time but rather during the day. Fig. 5 shows that the UWI becomes less negative after this evening transition (between 20 and 22 UTC), but does not become positive.

The frequency distribution for the evening hours where the urban boundary layer is unstable and the rural boundary layer is already stable (Fig. 7), shows that the UWI for these transitional cases leans more towards negative values compared to the convective daytime values. The positive side of the distribution looks very similar however, though strongly positive values are absent. The total number of hours where this transition happens is also limited, 173 in total after filtering for high rain days (rain flag category 2), but even when including those days, the shape of the distribution changes only slightly, centring more around 0 and containing larger outliers. Nearly all days show this transition, which typically occurs between 18:00 and 20:00 UTC, i.e. around or a little after sunset. The UWI during this time shows no distinct difference from that of the entire dataset averaged. This means that the evening UWI is not strongly different in magnitude from the UWI formed during (convective) daytime.

However, when looking at the days where the maximum daily UWI happens during this evening time window, a pattern emerges (12 days in total). The UWI over the course of the day is generally positive or very close to zero, and at the end of the afternoon ($\sim$ 16:00 UTC) starts to increase to reach its maximum during the transition phase (Fig. 8a). This maximum UWI tends to be fairly high, over 2 ms^{-1} in half of the cases, and then shows a reduction as the night progresses and the urban PBL becomes stable. When taking the transition window somewhat wider, considering the daily maximum UWI between 18:00 and 23:00 UTC (23 days in total), the time evolution is similar, but the values are somewhat lower, with a more gradual decrease during night-time (Fig. 8b).

4.5. Role of initial conditions

The relation between initial PBL-depth and the magnitude of the UWI as found in *D18* seems to be much weaker in this dataset. Fig. 9 relates PBL-depth of urban and rural boundary layers at 4:00 UTC (6:00 LT, just after sunrise) to the maximum UWI during that day, but a clear pattern is not present. The higher UWI values (>2 ms^{-1}) all lie above the 1:1 line, so for situations with a higher initial urban than rural PBL depth. However, there are also plenty of low-UWI days in this area of the diagram, particularly for the very low values. The size of the points indicates the duration of the UWI episode of that day (i.e. consecutive hours with positive UWI values).

A higher urban PBL depth occasionally coincides with higher daily maximum UWI values, but there is no convincing relation: a statistical (non-parametric) test of the difference between the two data clusters above and below the 1:1 line yielded no significant difference. This is different from the *D18* study which showed a dependence on the initial PBL depth, which was especially strong for

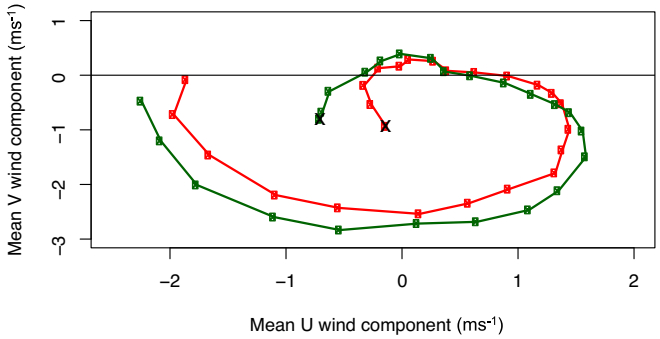

Fig. 6. Hodograph of modelled urban (red) and rural (green) mean hourly wind speed for selected days without rain (selection similar to Fig. 5). Each point represents one hour, starting at the crosses at 0:00 UTC and going counter-clockwise, ending at 23:00 UTC. The distance between the red and green line indicate the UWI. (For interpretation of the references to colour in this figure legend, the reader is referred to the web version of this article.)

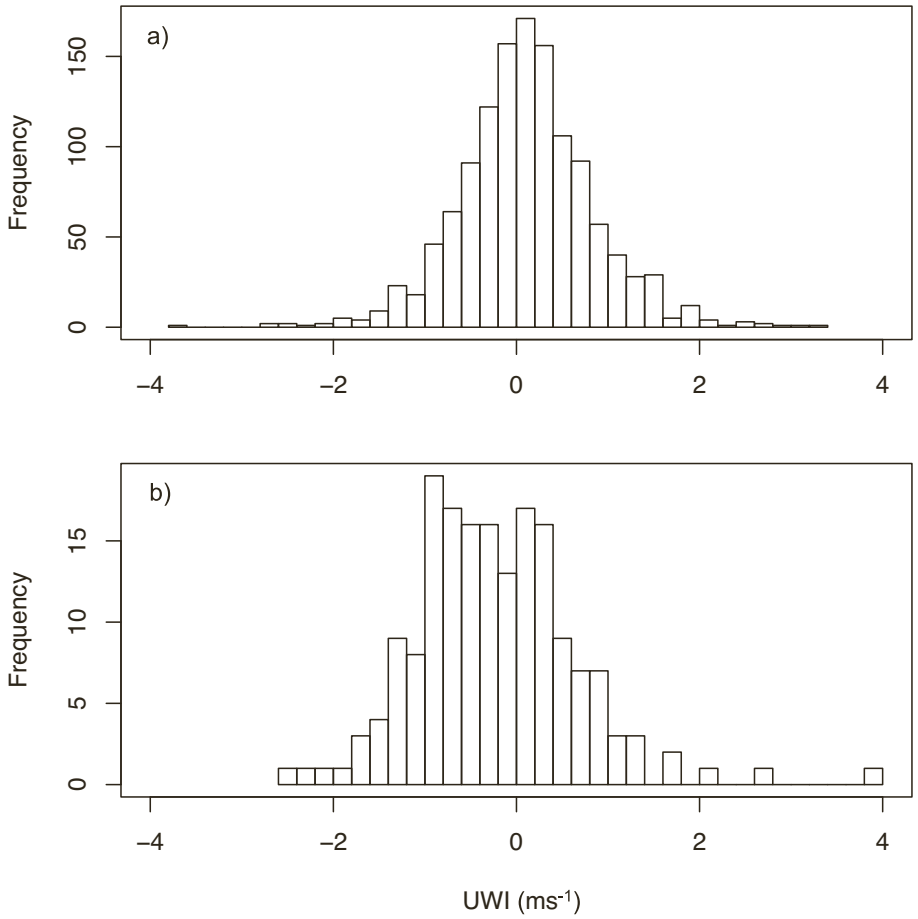

Fig. 7. Frequency distributions of the hourly modelled UWI where both urban and rural boundary-layers are unstable (upper panel) and where the urban PBL is still unstable where the rural PBL is already stable (lower panel).

days with a high initial difference between rural and urban boundary-layer depths. Such days do not seem to exist within this dataset, and might therefore not be very realistic for Amsterdam. A statistical extrapolation based on these data (not shown) does show a similar relation between UWI and PBL depth as in *D18*, but the required combination for PBL depths does not show up in this dataset, so that extrapolation cannot be reliably used.

In a similar fashion, the value of the geostrophic wind speed is a less dominant driver for the UWI formation than was apparent in *D18*. The relation with the initial ageostrophic wind ($U_{geo} - U_{PBL}$) at sunrise is weakly positive, where a larger difference between the boundary-layer wind speed and the geostrophic wind speed seems to lead to larger UWI values (results not shown). Exploring the daily mean geostrophic wind speed (Fig. 10), the relation between geostrophic wind and the daily maximum UWI is again not as clear-cut as for the conceptual model, though generally moderate geostrophic wind speeds coincide with higher UWI values. Interestingly, higher geostrophic wind correlates with the number of hours that a positive UWI does occur on a given day: especially within the 10–15 ms^{-1} geostrophic wind range. Why exactly this happens is unclear: potentially the higher geostrophic wind speed incites stronger boundary-layer flows that get accelerated through the enhanced urban turbulence.

5. Discussion

In this study we find that the UWI is convincingly present in the WRF model results, and not just in very specific circumstances, but even those that are not "typical" nice summer days. As such this supports the hypothesis that the UWI is a mechanism that occurs in real-world conditions. The mean value of the positive UWI over all studied summer days without rain amounts to 0.2 ms^{-1} (Fig. 5), while for an ideal day the UWI amounts to 0.5 ms^{-1} (Fig. 3). This is a similar order of magnitude as the conceptual model experiments of *D18*. The average diurnal UWI evolution, and the time-averaged hodograph in Figs. 5 and 6 correspond very well to the theoretical model results of the UWI as in *D18*, with an acceleration phase and positive UWI's during morning/early afternoon, and followed by negative values. The UWI timing on average is very similar to the *D18* work, with the onset a little earlier (few hours after sunrise), but the maximum UWI is also found in the afternoon. However, we recognize that individual days can strongly diverge from the average pattern, and reach substantially higher values, up to 3 ms^{-1}.

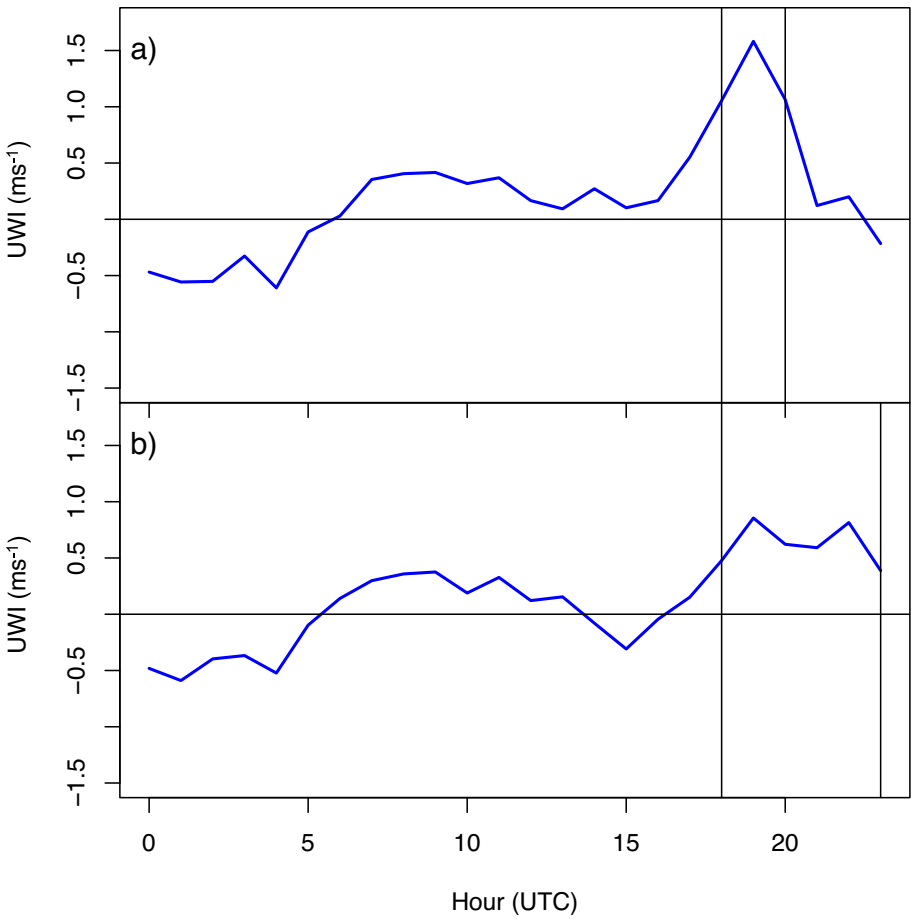

Fig. 8. Modelled UWI evolution for days with the maximum daily UWI between 18:00 UTC and 20:00 UTC (a) or 18:00 UTC and 23:00 UTC (b). Vertical black lines denote the time frame when the maximum daily UWI occurs, which coincides roughly with the evening transition of the PBL.

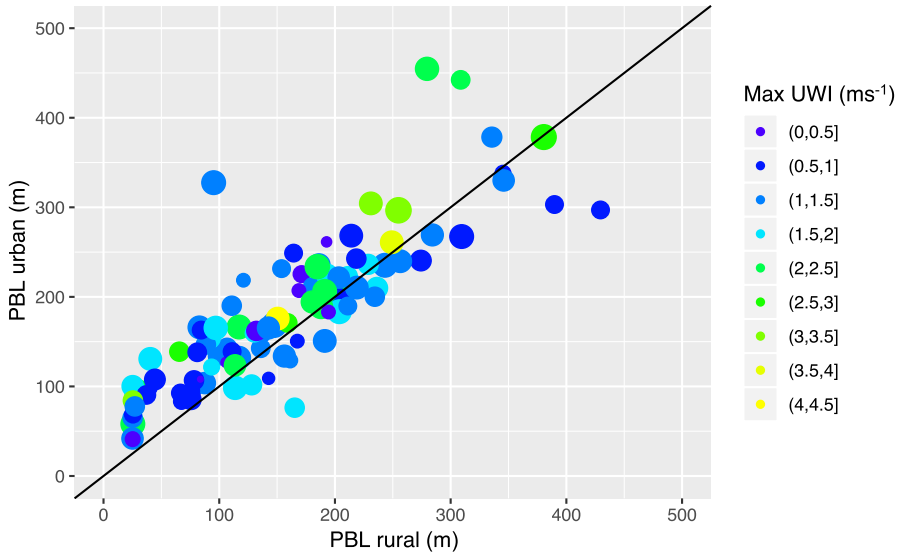

Fig. 9. Scatter plot of modelled daily rural and urban PBL depth at 4:00 UTC (6:00 LT) clustered according to the modelled maximum daily UWI (colours). The size of the points indicates the duration of a positive UWI episode of that day: consecutive positive UWI values.

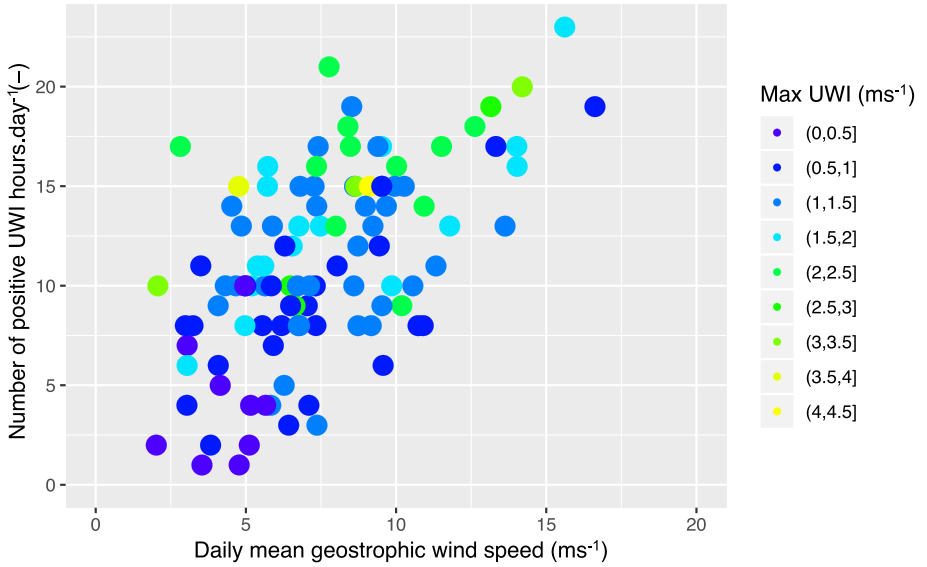

Fig. 10. Modelled daily mean geostrophic wind versus the number of positive UWI hours for a given day (with no to little rain). The coloured points indicate the value of the daily maximum UWI for that day.

Concerning the possible UWI development in the evening transition, we find that when the rural boundary layer reaches stable stratification earlier than the urban area, a UWI can form through the suppression of turbulence in the rural area while it persists in the city. This occurs typically a few hours around sunset (18:00–20:00 UTC). In these situations, the UWI increases at the end of the afternoon, peaking at around 19:00 UTC before reducing in value again as the night progresses and the urban boundary layer becomes (weakly) stable or neutral. This is a separate effect from the UWI caused by differences in the inertial oscillation of wind during the day, and typically leads to a weaker UWI that persists for a shorter period of time (∼ 2–3 h).

Overall the UWI's conceptual framework from *D18* broadly fits the UWI formation as seen in the more realistic WRF setting, but the importance of the difference in initial urban and rural PBL depth seems to play a smaller role. We find some relation between the PBL depth at the start of the day (4:00 UTC, corresponding to 6:00 LT as also used in *D18*), with a higher urban boundary layer typically leading to a higher maximum UWI, but not in all situations. The signal is somewhat noisier and not as clear-cut as the conceptual study. The magnitude of the geostrophic wind speed is seemingly an important component of the UWI formation in the conceptual study, but this relation is much less apparent and much noisier without any real pattern in the three-dimensional data. While a general relation is still visible, and similar to the conceptual study, we find quite some spread, but the number of positive UWI hours in a day seems to depend on the mean geostrophic wind speed.

In this analysis we have chosen for a area-averaged UWI, rather than a spatial analysis, mainly because the model infrastructure is too coarse to do detailed spatial analysis of this phenomenon. The definition of a UWI (or indeed a UHI) requires a background value, which necessarily is either a point or grid average, otherwise a meaningful UWI cannot be constructed. While we could construct a map of the UWI in Amsterdam, not much of value would be gained, since the length scales of urban heterogeneity are much smaller than the grid size of 500 m, so spatial variability would not be very valid, and could suggest spatial patterns that are perhaps not valid in a realistic urban setting.

Amsterdam is by international standards a relatively small city. The conceptual model in *D18* assumed separate urban and rural columns, with boundary-layer properties fully formed by these respective surfaces. Since Amsterdam is of limited size, the urban boundary layer might well have some rural advection changing its composition. Similarly, the land surrounding Amsterdam are also of mixed land-use, with various small towns interspersed with the natural areas. Repeating this study for larger cities, like megacities with distinct urban atmospheres might yield firmer results that could be closer to the conceptual model work. However, this will require substantially more computing capacity to apply the hectometric resolution used here.

While we have taken care to identify cases where larger-scale processes influence the wind pattern, it is possible that not all of these situations have been properly captured when constructing the long-period statistics. Amsterdam is located relatively close to the North Sea (∼30 km), and can experience sea breeze fronts in situations when the land-sea temperature contrast is sufficiently large. These fronts can reach either the rural or urban area at a different timing, resulting in large positive or negative wind differences which would suggest a UWI. Alternatively one could study the sudden changes in wind direction at either area, but this is no guarantee that a sea breeze front is actually passing, or that some other process, such as onset of stability (which is a local process we are interested in) is modifying wind direction.

Validation of the WRF model was primarily reported in (Tolk et al., 2009; Steeneveld et al., 2011) for the countryside and in (Ronda et al., 2017) for Amsterdam. However, the latter did not evaluate wind speed since the available urban canyon wind measurements are non-representative for a grid cell mean wind. Translation canyon wind speed observations to boundary-layer wind will occur with a

notable degree of error and is therefore omitted here. Future validation works could benefit from intensive field campaigns in which city and countryside are intensively monitored, including wind profiling with ground-based remote sensing (e.g. (Fenner et al., 2024)).

Analysis of longer datasets (e.g. the ERA-URBAN urban meteorology reanalysis project, (van Haren et al., 2018; Koopmans et al., 2023)), also encompassing multiple cities in different geographical situations, would solidify the statistics of this study. Amsterdam is surrounded by urban agglomerations and water bodies, which makes the selection of a good rural reference challenging. Moreover, a more theoretical case study in WRF, by creating an "academic city" (e.g. Theeuwes et al., 2013), could identify the influence of the forcings such as the geostrophic equilibrium and the PBL depth, especially since a statistical extrapolation does suggest a dependence on the initial PBL depth, but the data does not show the combination of PBL depths where this occurs.

Only a limited number of studies is available to compare current results with earlier modelling efforts and observations. Regional climate model simulations by (Karlický et al., 2020) revealed a wind reduction over cities that was smaller in summer than in other seasons. Although this result is not a pure UWI, it indicates a model response in the same direction as ours. Moreover, (Brandi et al., 2024) performed high-resolution WRF model simulations for Phoenix (U.S.A.) and did not find any UWI in their model results. However, the relatively dry countryside (low soil moisture) and moist city represents a landscape that is mirrored to the one studied here. Differences in PBL depth required for the UWI to form might not be reached in such a landscape. Interestingly (Oerlemans, 1967) developed a two-layer model for the urban heat island wind circulation that accounts for stratification and rotation. Although the model was developed to forecast air pollutant transport in the first place, the paper explored model results for various sets of characteristic atmospheric conditions (layer depth, stratification and rotation). In the case of relatively low stratification and deep boundary layers, which mimics the conditions favourable for the UWI in the current study, his model results produce overshooting of the upper-level wind speed, i.e. a similar behaviour as seen in our current model results. Hence the model by (Oerlemans, 1967) which is of intermediate complexity between the *D18* and WRF models, generates analogue model behaviour. Considering observations of the UWI, (Chandler, 1965) reported wind observations over London (U.K.) in which the urban wind speed was surprisingly higher in the city than in the countryside for conditions in which a mesoscale background wind was below a threshold of 4 ms^{-1}, combined with a relatively strong UHI effect. On the contrary, a later observational study by (Shreffler, 1979) for St. Louis (U.S.A.) reported also a UWI, though for weak UHI effects and calm mesoscale background winds. Such specific regimes were not found in our study, and as such this issue remains open for further study.

6. Conclusion

In this study we have investigated the so called Urban Wind Island (UWI), i.e. the phenomenon that the daytime boundary-layer mean wind speed in the city exceeds its counterpart in the countryside. While an earlier study in *D18* showed the principle behind the UWI in a bulk model for the boundary layer, here we confirm its existence in the setting of the three-dimensional mesoscale meteorological model WRF for the city of Amsterdam (The Netherlands). High resolution model results from two consecutive summers indicate that the UWI is clearly present in the context of a true city. Aside from a daytime UWI, model results also indicate the presence of an UWI in the evening, induced by the delayed transition to the stable nocturnal boundary layer in the city. Unlike the conceptual framework, a clear-sky convective day with low wind speeds that would be beneficial for the UHI is not required for the UWI, since we do not find a clear relation to radiation or the magnitude of the geostrophic wind, while days with little rain still generate a positive UWI.

Author statement

The model results and methodology used to obtain the data in this paper were originally developed by Ronda et al. (2017). Post processing and analysis of model results was performed by A.M. Droste with input from G.J. Steeneveld and A.A.M. Holtslag. The chapter was drafted by A.M. Droste and revised with input from G.J. Steeneveld and A.A.M. Holtslag, and all co-authors approved it for inclusion in this thesis.

CRediT authorship contribution statement

A.M. Droste: Writing – original draft, Software, Methodology, Investigation, Formal analysis, Conceptualization. **A.A.M. Holtslag:** Writing – review & editing, Supervision, Methodology, Conceptualization. **G.J. Steeneveld:** Writing – review & editing, Supervision, Methodology, Conceptualization.

Data availability

Data will be made available on request.

Acknowledgements

The authors would like to thank Hendrik Wouters for his input and help in conceiving the idea behind this paper; and Aristofanis Tsiringakis for his help in calculating the geostrophic wind speed from WRF. A.M. Droste and G.J. Steeneveld acknowledge funding from the Netherlands Organisation for Scientific Research (NWO) VIDI Grant 'The Windy City' (file no. 864.14.007). We also knowledge funding from NWO grant SH-312-15 (computing hours).

References

Azargoshasbi, F., Ashrafi, K., Ehsani, A.H., 2023. Role of urban boundary layer dynamics and ventilation efficiency in a severe air pollution episode in Tehran, Iran. Meteorog. Atmos. Phys. 135, 35. https://doi.org/10.1007/s00703-023-00972-3.

Barlow, J.F., 2014. Progress in observing and modelling the urban boundary layer. Urban Clim. 10, 216–240. https://doi.org/10.1016/j.uclim.2014.03.011 iCUC8: The 8th International Conference on Urban Climate and the 10th Symposium on the Urban Environment.

Barlow, J., Best, M., Bohnenstengel, S.I., Clark, P., Grimmond, S., Lean, H., Christen, A., Emeis, S., Haeffelin, M., Harman, I.N., Lemonsu, A., Martilli, A., Pardyjak, E., Rotach, M.W., Ballard, S., Boutle, I., Brown, A., Cai, X., Carpentieri, M., Coceal, O., Crawford, B., Sabatino, S.D., Dou, J., Drew, D.R., Edwards, J.M., Fallmann, J., Fortuniak, K., Gornall, J., Gronemeier, T., Halios, C.H., Hertwig, D., Hirano, K., Holtslag, A.A.M., Luo, Z., Mills, G., Nakayoshi, M., Pain, K., Schlünzen, K.H., Smith, S., Soulhac, L., Steeneveld, G.-J., Sun, T., Theeuwes, N.E., Thomson, D., Voogt, J.A., Ward, H.C., Xie, Z.-T., Zhong, J., 2017. Developing a research strategy to better understand, observe, and simulate urban atmospheric processes at kilometer to subkilometer scales. Bull. Am. Meteorol. Soc. 98. ES261 – ES264. URL: https://journals.ametsoc.org/view/journals/bams/98/10/bams-d-17-0106.1.xml https://doi.org/10.1175/BAMS-D-17-0106.1.

Bassett, R., Cai, X., Chapman, L., Heaviside, C., Thornes, J.E., 2019. Semi-idealized urban heat advection simulations using the weather research and forecasting mesoscale model. Int. J. Climatol. 39, 1345–1358. URL: http://doi.wiley.com/10.1002/joc.5885 https://doi.org/10.1002/joc.5885.

Biehl, J.L., Paas, B., Klemm, O., 2021. Ventilation of a mid-size city under stable boundary layer conditions: a simulation using the les model palm. Atmosphere 12. URL: https://www.mdpi.com/2073-4433/12/3/401 https://doi.org/10.3390/atmos12030401.

Blackadar, A.K., 1957. Boundary layer wind maxima and their significance for the growth of nocturnal inversions. Bull. Am. Meteorol. Soc. 38, 283–290.

Bornstein, R.D., Johnson, D.S., 1967. Urban-rural wind velocity differences. Atmos. Environ. 11 (1977), 597–604. https://doi.org/10.1016/0004-6981(77)90112-3.

Brandi, A., Martilli, A., Salamanca, F., Georgescu, M., 2024. Urban boundary-layer flows in complex terrain: dynamic interactions during a hot and dry summer season in phoenix, arizona. Q. J. R. Meteorol. Soc. 150, 3099–3116. URL: https://rmets.onlinelibrary.wiley.com/doi/abs/10.1002/qj.4752. doi:10.1002/qj.4752.

Byun, D.W., Arya, S.P.S., 1967. A study of mixed-layer momentum evolution. Atmos. Environ. 20 (1986), 715–728. https://doi.org/10.1016/0004-6981(86)90186-1.

Chandler, T., 1965. The Climate of London, Atmospheric Environment (1967).

Chen, F., Kusaka, H., Bornstein, R., Ching, J., Grimmond, C.S.B., Grossman-Clarke, S., Loridan, T., Manning, K.W., Martilli, A., Miao, S., Sailor, D., Salamanca, F.P., Taha, H., Tewari, M., Wang, X., Wyszogrodzki, A.A., Zhang, C., 2011. The integrated wrf/urban modelling system: development, evaluation, and applications to urban environmental problems. Int. J. Climatol. 31, 273–288. https://doi.org/10.1002/joc.2158.

Droste, A.M., Steeneveld, G.J., Holtslag, A.A.M., 2018. Introducing the urban wind island effect. Environ. Res. Lett. 13, 094007. URL: http://stacks.iop.org/1748-9326/13/i=9/a=094007?key=crossref.20cecdb1bbb8739c7811dedbf48bc43b https://doi.org/10.1088/1748-9326/aad8ef.

Ek, M.B., Mitchell, K.E., Lin, Y., Rogers, E., Grunmann, P., Koren, V., Gayno, G., Tarpley, J.D., 2003. Implementation of noah land surface model advances in the national centers for environmental prediction operational mesoscale eta model. J. Geophys. Res. Atmos. 108. https://doi.org/10.1029/2002JD003296.

Fallmann, J., Forkel, R., Emeis, S., 2016. Secondary effects of urban heat island mitigation measures on air quality. Atmos. Environ. 125, 199–211. URL: https://www.sciencedirect.com/science/article/pii/S1352231015305094 https://doi.org/10.1016/j.atmosenv.2015.10.094.

Fenner, D., Christen, A., Grimmond, S., Meier, F., Morrison, W., Zeeman, M., Barlow, J., Birkmann, J., Blunn, L., Chrysoulakis, N., Clements, M., Glazer, R., Hertwig, D., Kotthaus, S., König, K., Looschelders, D., Mitraka, Z., Poursanidis, D., Tsirantonakis, D., Bechtel, B., Benjamin, K., Beyrich, F., Briegel, F., Feigel, G., Gertsen, C., Iqbal, N., Kittner, J., Lean, H., Liu, Y., Luo, Z., McGrory, M., Metzger, S., Paskin, M., Ravan, M., Ruhtz, T., Saunders, B., Scherer, D., Smith, S.T., Stretton, M., Trachte, K., M. V., 2024. Hove, urbisphere-berlin campaign: investigating multi-scale urban impacts on the atmospheric boundary layer. Bull. Am. Meteorol. Soc. URL: https://journals.ametsoc.org/view/journals/bams/aop/BAMS-D-23-0030.1/BAMS-D-23-0030.1.xml https://doi.org/10.1175/BAMS-D-23-0030.1.

Fortuniak, K., Kłysik, K., Wibig, J., 2006. Urban–rural contrasts of meteorological parameters in Łódź. Theor. Appl. Climatol. 84, 91–101. URL: https://link.springer.com/content/pdf/10.1007%2Fs00704-005-0147-y.pdf https://doi.org/10.1007/s00704-005-0147-y.

Hong, S.-Y., Lim, J.-O.J., 2012. The wrf single-moment 6-class microphysics scheme (wsm6). J. Korean Meteorol. Soc. 42, 29–151. https://doi.org/10.1175/MWR-D-11-00056.1.

Hong, S.-Y., Noh, Y., Dudhia, J., 2006. A new vertical diffusion package with an explicit treatment of entrainment processes. Mon. Weather Rev. 134, 2318–2341. https://doi.org/10.1175/MWR3199.1.

Iacono, M.J., Delamere, J.S., Mlawer, E.J., Shephard, M.W., Clough, S.A., Collins, W.D., 2008. Radiative forcing by long-lived greenhouse gases: calculations with the aer radiative transfer models. J. Geophys. Res. Atmos. 113. https://doi.org/10.1029/2008JD009944.

Jiménez, P.A., Dudhia, J., González-Rouco, J.F., Navarro, J., Montávez, J.P., García-Bustamante, E., 2012. A revised scheme for the wrf surface layer formulation. Mon. Weather Rev. 140, 898–918. https://doi.org/10.1175/MWR-D-11-00056.1.

Jing, Y., Zhong, H.-Y., Wang, W.-W., He, Y., Zhao, F.-Y., Li, Y., 2021. Quantitative city ventilation evaluation for urban canopy under heat island circulation without geostrophic winds: multi-scale cfd model and parametric investigations. Build. Environ. 196, 107793. URL: https://www.sciencedirect.com/science/article/pii/S0360132321002006 https://doi.org/10.1016/j.buildenv.2021.107793.

Kain, J.S., 2004. The kain–fritsch convective parameterization: an update. J. Appl. Meteorol. 43, 170–181. https://doi.org/10.1175/1520-0450(2004)043<0170:TKCPAU>2.0.CO;2.

Karlický, J., Huszár, P., Halenka, T., Belda, M., Žák, M., Pišoft, P., Mikšovský, J., 2018. Multi-model comparison of urban heat island modelling approaches. Atmos. Chem. Phys. 18, 10655–10674. URL: https://acp.copernicus.org/articles/18/10655/2018/ https://doi.org/10.5194/acp-18-10655-2018.

Karlický, J., Huszár, P., Nováková, T., Belda, M., Švábik, F., Ďoubalová, J., Halenka, T., 2020. The "urban meteorology island": a multi-model ensemble analysis. Atmos. Chem. Phys. 20, 15061–15077. URL: https://acp.copernicus.org/articles/20/15061/2020/ https://doi.org/10.5194/acp-20-15061-2020.

Koopmans, S., van Haren, R., Theeuwes, N., Ronda, R., Uijlenhoet, R., Holtslag, A.A.M., Steeneveld, G.-J., 2023. The set-up and evaluation of fine-scale data assimilation for the urban climate of Amsterdam. Q. J. R. Meteorol. Soc. 149, 171–191. https://doi.org/10.1002/qj.4401.

Koracin, D., Berkowicz, R., 1988. Nocturnal boundary-layer height: observations by acoustic sounders and predictions in terms of surface-layer parameters. Bound.-Layer Meteorol. 43, 65–83. URL: http://link.springer.com/10.1007/BF00153969 https://doi.org/10.1007/BF00153969.

Lee, D., 1967. The influence of atmospheric stability and the urban heat island on urban-rural wind speed differences. Atmos. Environ. 13 (1979), 1175–1180. https://doi.org/10.1016/0004-6981(79)90042-8.

Micallef, D., Bussel, G.V., 2018. A review of urban wind energy research: aerodynamics and other challenges. Energies 11. URL: https://www.mdpi.com/1996-1073/11/9/2204 https://doi.org/10.3390/en11092204.

Nazarian, N., Krayenhoff, E.S., Bechtel, B., Hondula, D.M., Paolini, R., Vanos, J., Cheung, T., Chow, W.T.L., de Dear, R., Jay, O., Lee, J.K.W., Martilli, A., Middel, A., Norford, L.K., Sadeghi, M., Schiavon, S., Santamouris, M., 2022. Integrated assessment of urban overheating impacts on human life. Earth's Future 10 e2022EF002682. URL: https://agupubs.onlinelibrary.wiley.com/doi/abs/10.1029/2022EF002682 https://doi.org/10.1029/2022EF002682. arXiv.

Oerlemans, J., 1967. Linear theory of the urban heat island circulation. Atmos. Environ. 20 (1986), 447–453. URL: https://www.sciencedirect.com/science/article/pii/0004698186900843 https://doi.org/10.1016/0004-6981(86)90084-3.

Oke, T.R., Mills, G., Christen, A., Voogt, J.A., 2017. Urban Climates. Cambridge University Press.

Powers, J.G., Klemp, J.B., Skamarock, W.C., Davis, C.A., Dudhia, J., Gill, D.O., Coen, J.L., Gochis, D.J., Ahmadov, R., Peckham, S.E., Grell, G.A., Michalakes, J., Trahan, S., Benjamin, S.G., Alexander, C.R., Dimego, G.J., Wang, W., Schwartz, C.S., Romine, G.S., Liu, Z., Snyder, C., Chen, F., Barlage, M.J., Yu, W., Duda, M.G., 2017. The weather research and forecasting model: overview, system efforts, and future directions. Bull. Am. Meteorol. Soc. 98, 1717–1737. URL: http://journals.ametsoc.org/doi/10.1175/BAMS-D-15-00308.1 https://doi.org/10.1175/BAMS-D-15-00308.1.

Ronda, R.J., Steeneveld, G.J., Heusinkveld, B.G., Attema, J., Holtslag, A.A.M., 2017. Urban finescale forecasting reveals weather conditions with unprecedented detail. Bull. Am. Meteorol. Soc. 98, 2675–2688. https://doi.org/10.1175/BAMS-D-16-0297.1.

Shreffler, J.H., 1979. Urban-rural differences in tower-measured winds, st. louis. J. Appl. Meteorol. Climatol. 18, 829–835. URL: https://journals.ametsoc.org/view/journals/apme/18/7/1520-0450_1979_018_0829_urditm_2_0_co_2.xml. doi:10.1175/1520-0450(1979)018<0829:URDITM>2.0.CO;2.

Skamarock, W.C., Klemp, J.B., Dudhia, J., Gill, D.O., Barker, D.M., Duda, M.G., Huang, X.-Y., Wang, W., Powers, J.G., 2008. A Description of the Advanced Research WRF Version 3, Technical Report NCAR/TN–475+STR. NCAR.

Sluiter, R., 2011. Klimaatatlas. URL: http://www.klimaatatlas.nl/.

Steeneveld, G.J., van de Wiel, B.J.H., Holtslag, A.A.M., 2007. Diagnostic equations for the stable boundary layer height: evaluation and dimensional analysis. J. Appl. Meteorol. Climatol. 46, 212–225. URL: http://journals.ametsoc.org/doi/10.1175/JAM2454.1 https://doi.org/10.1175/JAM2454.1.

Steeneveld, G.J., Tolk, L.F., Moene, A.F., Hartogensis, O.K., Peters, W., Holtslag, A.A.M., 2011. Confronting the wrf and rams mesoscale models with innovative observations in the Netherlands: evaluating the boundary layer heat budget. J. Geophys. Res. Atmos. 116. https://doi.org/10.1029/2011JD016303.

Stull, R.B., 1988. An Introduction to Boundary Layer Meteorology. Springer, Netherlands. https://doi.org/10.1007/978-94-009-3027-8.

Theeuwes, N.E., Solcerová, A., Steeneveld, G.J., 2013. Modeling the influence of open water surfaces on the summertime temperature and thermal comfort in the city. J. Geophys. Res. Atmos. 118, 8881–8896. https://doi.org/10.1002/jgrd.50704.

Tolk, L.F., Peters, W., Meesters, A.G.C.A., Groenendijk, M., Vermeulen, A.T., Steeneveld, G.J., Dolman, A.J., 2009. Modelling regional scale surface fluxes, meteorology and co_2 mixing ratios for the cabauw tower in the Netherlands. Biogeosciences 6, 2265–2280. URL: https://bg.copernicus.org/articles/6/2265/2009/ https://doi.org/10.5194/bg-6-2265-2009.

Tsiringakis, A., Theeuwes, N.E., Barlow, J.F., Steeneveld, G.-J., 2022. Interactions between the nocturnal low-level jets and the urban boundary layer: a case study over London. Bound.-Layer Meteorol. 183, 249–272. https://doi.org/10.1007/s10546-021-00681-7.

U. N. D. of Economic, S. Affairs, Urban and Rural Population Growth and World Urbanization Prospects. World Urbanization Prospects: The, 2018. Revision, Technical Report. United Nations Department of Economic and Social Affairs, p. 2019.

van de Wiel, B.J.H., Moene, A.F., Steeneveld, G.J., Baas, P., Bosveld, F.C., Holtslag, A.A.M., 2010. A conceptual view on inertial oscillations and nocturnal low-level jets. J. Atmos. Sci. 67, 2679–2689. https://doi.org/10.1175/2010JAS3289.1.

van Haren, R., Koopmans, S., Steeneveld, G.-J., Theeuwes, N., Uijlenhoet, R., Holtslag, A.A., 2018. Weather reanalysis on an urban scale using wrf. In: 2018 IEEE 14th International Conference on e-Science (e-Science), pp. 279–280. https://doi.org/10.1109/eScience.2018.00049.

Vogelezang, D.H.P., Holtslag, A.A.M., 1996. Evaluation and model impacts of alternative boundary-layer height formulations. Bound.-Layer Meteorol. 81, 245–269. https://doi.org/10.1007/BF02430331.

Wallace, J.M., Hobbs, P.V., 2006. Atmospheric Science. Elsevier. https://doi.org/10.1016/C2009-0-00034-8.

Yang, Y.-J., Wu, B.-W., Eshi, C., Zhang, J.-H., Li, Y.-B., Tang, W.-A., Wen, H.-Y., Zhang, H.-Q., Shi, T., 2013. Impacts of urbanization and station-relocation on surface air temperature series in Anhui province, China. Pure Appl. Geophys. 170, 1969–1983. https://doi.org/10.1007/s00024-012-0619-9.

Zhang, X., Han, L., Wei, H., Tan, X., Zhou, W., Li, W., Qian, Y., 2022. Linking urbanization and air quality together: a review and a perspective on the future sustainable urban development. J. Clean. Prod. 346, 130988. URL: https://www.sciencedirect.com/science/article/pii/S0959652622006230 https://doi.org/10.1016/j.jclepro.2022.130988.